

PACS numbers: 52.50.Jm; 52.57.Bc; 61.43.Hv
DOI: 10.1070/QE2015v045n06ABEH015625

Alpha-spectrometry and fractal analysis of surface micro-images for characterisation of porous materials used in manufacture of targets for laser plasma experiments

A.A. Aushev, S.P. Barinov, M.G. Vasin, Yu.M. Drozdov, Yu.V. Ignatev, V.M. Izgorodin, D.K. Kovshov, A.E. Lahtikov, D.D. Lukovkina, V.V. Markelov, A.P. Morovov, V.V. Shishlov

Abstract. **We present the results of employing the alpha-spectrometry method to determine the characteristics of porous materials used in targets for laser plasma experiments. It is shown that the energy spectrum of alpha-particles, after their passage through porous samples, allows one to determine the distribution of their path length in the foam skeleton. We describe the procedure of deriving such a distribution, excluding both the distribution broadening due to statistical nature of the alpha-particle interaction with an atomic structure (straggling) and hardware effects. The fractal analysis of micro-images is applied to the same porous surface samples that have been studied by alpha-spectrometry. The fractal dimension and size distribution of the number of the foam skeleton grains are obtained. Using the data obtained, a distribution of the total foam skeleton thickness along a chosen direction is constructed. It roughly coincides with the path length distribution of alpha-particles within a range of larger path lengths. It is concluded that the combined use of the alpha-spectrometry method and fractal analysis of images will make it possible to determine the size distribution of foam skeleton grains (or pores). The results can be used as initial data in theoretical studies on propagation of the laser and X-ray radiation in specific porous samples.**

Keywords: *targets for laser plasma studies, porous materials, alpha-spectrometry, fractal analysis of surface.*

1. Introduction

Many laboratories around the world conduct studies on the interaction of intense laser radiation with low density (porous) materials [1–3]. This is due to the opportunity of employing the plasma of porous media for smoothing the irregularities in irradiation of targets [4–12], for increasing the plasma temperature and efficiency of laser radiation conversion into X-ray radiation compared to the case of using the same material with normal density [13–16], and, finally, for controlling the spectral composition and creating coherent X-ray radiation sources. Furthermore, the use of porous media allows simulation of astrophysical phenomena in laboratory conditions and carrying out research on the properties and states of matter under dynamic loads at a pressure of a few megabars [17].

For explaining the experimental data and designing targets made of porous materials in order to obtain the desired effects (smoothing the irregularities, increasing the plasma temperature, etc.), knowledge of the foam characteristics is required. These characteristics include average density, optical density, geometrical thickness, pore size distribution, path length distribution of optical beams by their lengths in a material, etc. Currently, the main method of registration consists in a qualitative analysis of the microphotographs taken by means of an optical or electron microscope [2, 3]. More seldom, the foam structure representation in the approximation of fractal clusters [18, 19] is employed for microphotograph processing. To characterise the low-density films from a substance with a high atomic charge Z, the X-ray inspection methods are being developed [20].

Previously, Izgorodin et al. [21] noted the possibility of detecting cracks, damages or density irregularities in film samples of normal and low-density materials by means of alpha-spectrometry. These defects lead to a change in the energy spectrum of the alpha-particle beam after its passage through the sample. As a result, the spectra allow one to derive the path length distribution of alpha-particles in the skeleton of a porous sample and to draw certain conclusions as to the pore size distribution.

In this paper we present an experimental study on the application of alpha-spectrometry to determine the structure of porous film-type samples. Besides, an attempt is made to describe the structure of porous samples by means of relevant microphotographs in the approximation of fractal clusters and to relate the results of the fractal analysis with those obtained by alpha-spectrometry. All studies are performed with organic glass samples.

2. Use of alpha-spectrometry to determine the parameters of porous samples

To study the relation between the main characteristic of the alpha-particle beam – the energy spectrum – and the film parameters, we studied experimentally the passage of alpha-particles through film samples made of organic glass ($C_5H_8O_2$). Alpha-particles lose their energy when moving through a medium and their path length can be evaluated from the magnitude of energy losses. If the medium is not solid and has some voids, the energy of the particles having passed through the medium is dependent on their trajectories. Thus, in measuring the alpha-particle spectrum, we transform

A.A. Aushev, S.P. Barinov, M.G. Vasin, Yu.M. Drozdov, Yu.V. Ignatev, V.M. Izgorodin, D.K. Kovshov, A.E. Lahtikov, D.D. Lukovkina, V.V. Markelov, A.P. Morovov, V.V. Shishlov
Russian Federal Nuclear Center 'All Russian Research Institute of Experimental Physics', prosp. Mira 37, 607190 Sarov, Nizhnii Novgorod region, Russia, e-mail: vizgorodin@yandex.ru

Received 14 July 2014; revision received 05 September 2014
Kvantovaya Elektronika **45** (6) 533–539 (2015)
Translated by M.A. Monastyrskiy

the pore size distribution in a medium into the energy distribution of particles. However, the situation is complicated by the fact that, due to the atomic structure of matter, energy losses possess a statistical nature and the spectrum of the particles passed through the medium is broadened. This phenomenon is called straggling [22, 23]. In addition, the recorded spectrum is affected by the hardware broadening, non-parallelism of alpha-particle trajectories in the beam, and original source spectrum. Therefore, all these factors should be taken into account to highlight the contribution of pores in a medium.

2.1. Experimental setup

The spectra of the samples were measured using a spectrometer comprising a silicon surface barrier detector of the PD series (Detector PD100-12-300AM), a Model 2003BT preamplifier (Canberra), spectrometric modular-type NIM-standard equipment (Canberra), and a Multiport II digital signal analyser. The data from the digital signal analyser are fed into the processing computer. Accumulation and processing of the spectra are carried out using the Genie software. The detector and preamplifier are constructively combined into a single unit placed in a vacuum chamber. The energy resolution for the alpha particles with an energy of 5 MeV amounts to about 11 keV.

A schematic of sample measurements is presented in Fig. 1. A standard spectrometric source of Pu-238 alpha radiation is used as a source of alpha-particles. The emission spectrum of Pu-238 consists of two lines with the alpha-particle energies of 5499 and 5456 keV at a relative intensity of 70.9% and 29%, respectively. The active region of the source represents a round spot of 1 cm^2 in area, located at the metal substrate's centre. The diameter of the samples constitutes 5–6 mm. All measurements are performed in vacuum ($p \sim 10^{-2}$ mm Hg). The number of measuring channels reaches 16384; the energy width of the channel is ~0.4 keV. Control experiments aimed at determining the changes in spectrometric channel characteristics over time have shown that the drift of the energy distribution maximum in the course of 4 h turns out less than 10 analyser channels (less than 4 keV), which lies within the spectrometer energy resolution. Six samples of 0.014–0.016-cm-thick porous organic glass plates are used in the measurements. The plates are cut from a single piece of foam in three mutually perpendicular directions. The gravimetrically determined average density is equal to 0.092 g cm^{-3}. Figure 2 shows the energy spectrum of alpha-particles after passing through one of the samples of 0.015-cm-thick porous organic glass.

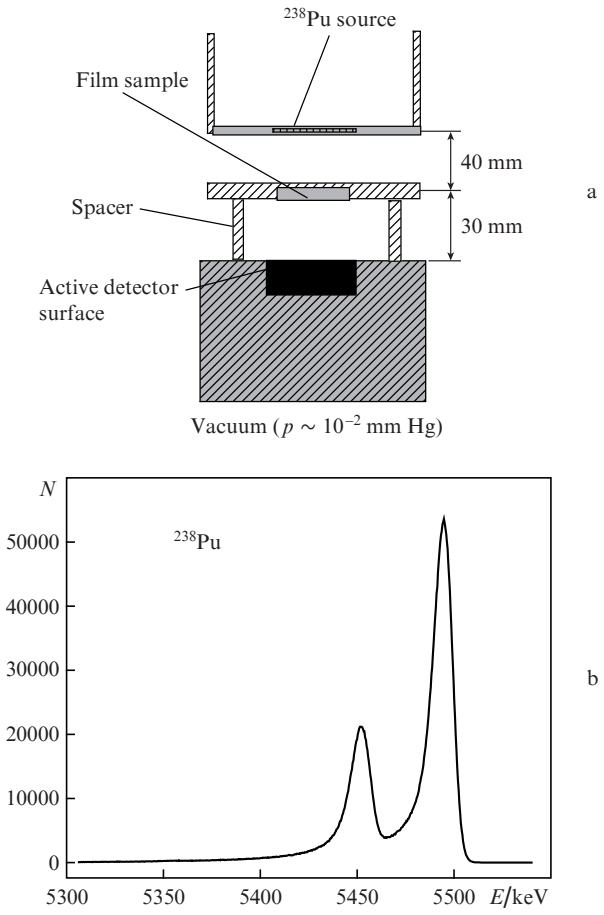

Figure 1. (a) Scheme of registration and (b) alpha-particle source spectrum.

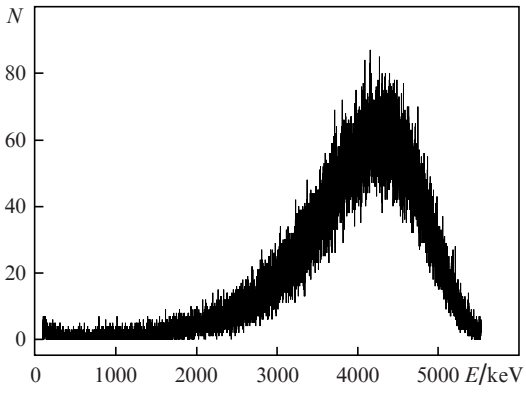

Figure 2. Energy spectrum of alpha-particles passed through a porous sample.

2.2. Processing of the alpha-particle spectrum

There is no doubt that a broad energy spectrum is mainly conditioned by a large variety of the path lengths of alpha-particles in the skeleton of foams. However, to distinguish the explicit contribution of pores (or foam skeleton) and build up the path length distribution of the alpha-particles in the sample structure, it is necessary to transform the experimental spectrum so as to eliminate the effect of all other relevant factors mentioned above. This procedure of spectrum processing is carried for all six samples.

The density of the path length distribution of alpha-particles in the skeleton, s, for the entire area of a porous sample is determined by the expression [24]

$$\varphi(s) = \int_0^\infty p_s(s/E)\psi_E(E)\,\mathrm{d}E, \tag{1}$$

where $p_s(s/E)$ is the conditional density of the path length distribution in the skeleton for the alpha-particles having the energy E after passing through the foam; and $\psi_E(E)$ is the experimental energy spectrum of alpha-particles after passing through the foam-type sample. Since the alpha-particle trajectories in the z-direction are randomly located in the xy plane, this distribution can be treated as a foam distribution

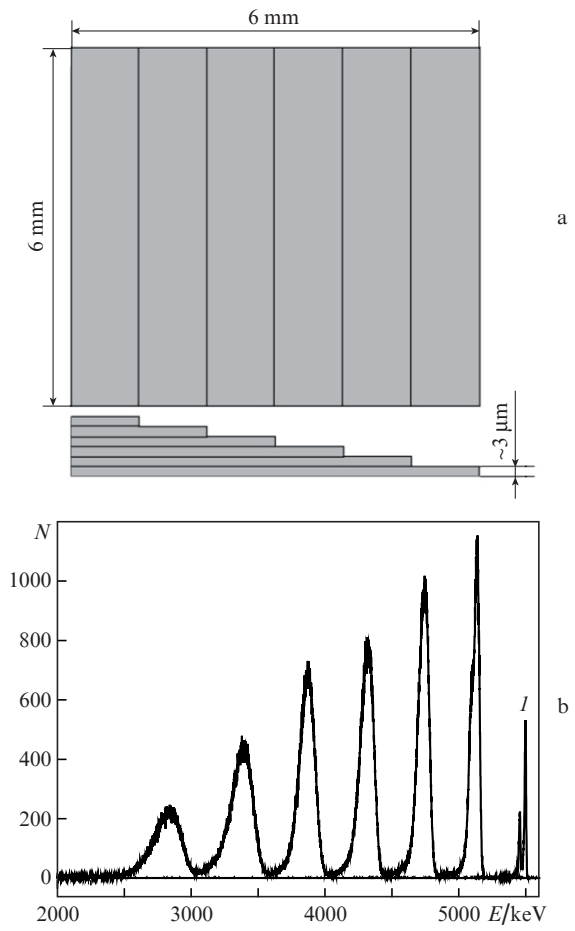

Figure 3. (a) Schematic of the assembly of six continuous films and (b) alpha-particle spectrum after passing through the sample. Curve (*1*) is the alpha-particle source peak.

by the skeleton thickness in the z-axis direction. The value of $p_s(s/E)$ is determined according to the Bayes formula

$$p_s(s/E) = \frac{\eta(s)p_\eta(E/s)}{\int_0^\infty p_\eta(E/s)\eta(s)\,\mathrm{d}s}, \tag{2}$$

where $\eta(s)$ is the density of the path length distribution for a solid sample in the selected direction; and $p_\eta(E/s)$ is the conditional density of the energy distribution of alpha-particles after passing the distance s in a solid sample. Taking into account that the path length distribution in a solid non-porous sample $\eta(s) = \text{const}$, we obtain

$$p_s(s/E) = \frac{p_\eta(E/s)}{\int_0^\infty p_\eta(E/s)\,\mathrm{d}s}. \tag{3}$$

Numerical calculation of the distribution density $p_\eta(E/s)$, with straggling, alpha-source spectrum, and hardware broadening taken into account, represents a complicated problem. This is the reason why the distribution $p_\eta(E/s)$ has been derived experimentally, by means of measuring the energy spectrum of the alpha-particles passed through a step-wise film-type sample from the solid material. The sample is composed of six superposed films of equal thickness (3 μm) as shown in Fig. 3a. The energy spectrum of alpha-particles, after their passing through such a sample, constitutes six peaks, the maxima of which on the energy scale are located in accordance with the average energy losses of the particles passed through one, two, and so on, solid films (Fig. 3b).

The shape of the function $p_\eta(E/s)$ is chosen from the following considerations. Firstly, the source spectrum has two well-pronounced peaks. In addition, the spectrum broadening caused by straggling is, generally speaking, asymmetrical relative to the maximum. Therefore, the spectrum peaks can be represented as a sum of two log-normal distributions:

$$p_\eta(E/s) = \frac{1}{\sqrt{2\pi}\,E'}\left\{\frac{1}{\sigma_1}\exp\left[-\frac{1}{2}\left(\frac{\ln E' - \ln E'_{\mathrm{m1}}}{\sigma_1}\right)^2\right]\right.$$

$$\left. + \frac{1}{\sigma_2}\exp\left[-\frac{1}{2}\left(\frac{\ln E' - \ln E'_{\mathrm{m2}}}{\sigma_2}\right)^2\right]\right\}, \tag{4}$$

where $E' = E_0 - E$, $E'_{\mathrm{m1,m2}} = E_0 - E_{\mathrm{m1,m2}}$, and $E_0 = \text{const}$ for the same experimental conditions; and $E_{\mathrm{m1,m2}}$ and $\sigma_{1,2}$ are functions of s. Figure 4 shows the families of distributions $p_\eta(E/s)$ [expression (4)] and $p_s(s/E)$ [expression (3)], which, with the use of formula (1), determine the distribution density by the skeleton thickness in the porous sample along the z-axis direction. This distribution is presented below in Fig. 9 [curve (*1*)]. In the calculations, the value of E_0 is taken equal to 5500 keV (position of the source peak).

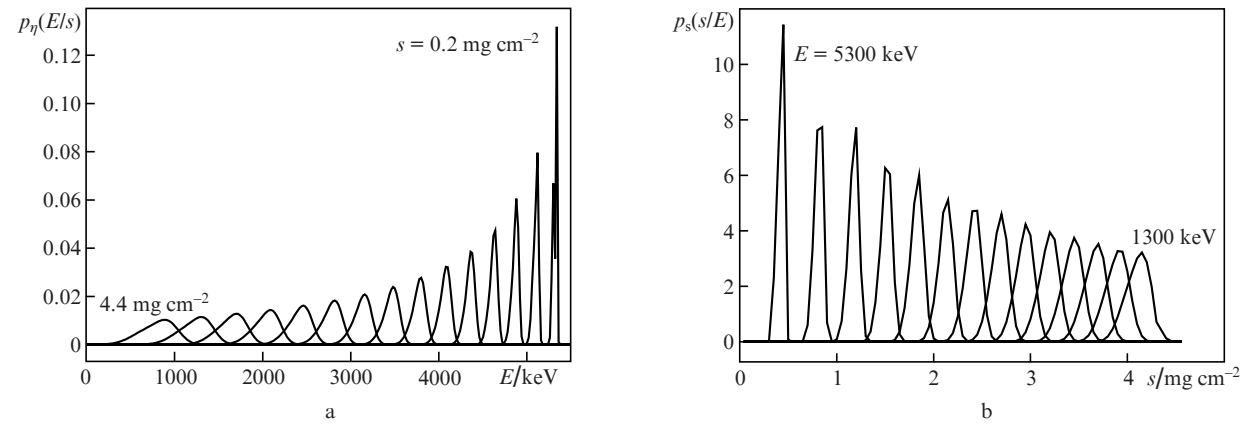

Figure 4. Family of curves $p_\eta(E/s)$ (a) for two optical path lengths and $p_s(E/s)$ (b) for two alpha-particle energy values.

The foam skeleton thickness distribution in the porous sample may also be obtained by the expression

$$\varphi_a(s) = \int_{E_s}^{E_0} (dE/ds)^{-1} \psi_E(E)\, dE, \quad (5)$$

where E_s is the alpha-particle energy at the final point of the trajectory having the length s; dE/dx is the stopping ability of the sample substance; and $\psi_E(E)$ is the experimental spectrum of the porous sample (Fig. 3). The distribution $\varphi_a(s)$ does not take into account the contribution of straggling and hardware broadening of thespectrum; it is also reproduced below in Fig. 9 [curve (*2*)]. It can be seen that, in the absence of corrections for straggling, hardware broadening, and source spectrum, this distribution differs from that obtained with such corrections. This is mainly due to the asymmetry of broadening. If straggling and source spectrum are Gaussian, this difference is negligibly small.

3. Fractal analysis of micro-images of the surfaces of porous samples

In nature, pure geometric fractals do not exist. As applied to porous structures, the use of fractal analysis is limited by crushing the parts – the pore size cannot exceed the size of the sample and the minimum size of the skeleton grain cannot be smaller than the size of the atom. Therefore, the fractal structure concept can only be used within certain limits. We have applied a relevant concept of fractal scaling [19, 25, 26] for analysis of the microphotographs of the same surfaces of porous samples that were studied by alpha-spectrometry.

3.1. Micro-images of the surface of porous samples

The microphotographs were obtained with a scanning electron microscope. Prior to analysis, the samples were covered with a 20-nm-thick gold layer. To reduce the radiation effect of the scanning electron beam on the structure, the samples were examined in a moderate regime of the electron probe: at the anode voltage of 7 kV and electron current in the beam of ~10 pA. The images of the near-surface structure were obtained with a magnification in the range from 30× to 10000×. Fig. 5 shows the microphotographs of the surface at the sample centre with three different magnifications. It can be seen that the structure is formed by the film-type elements – membranes – having a thickness from a few tens to hundreds of nanometres.

3.2. Determination of fractal dimension

The fractal dimension was determined by the method of 'areas' [18, 19] with the use of a special computer program of image processing. The noise was manually removed from the images prior to processing. The process of finding the dimension can be divided into two stages.

At the first stage, the original image, initially obtained in grey gradations, was converted into an image with two colours only – black and white. To do this, the average brightness over the entire image was determined by the formula

$$I = \frac{\sum_i^M n_i i}{M}, \quad (6)$$

where i is the brightness ranging from 0 (black) to 255 (white); n_i is the number of pixels in the image with a brightness i; and M is the number of pixels in the image (in our case 768 × 768). When constructing a black-and-white image, all the pixels with the brightness less than I were regarded black, whilst the pixels with the brightness greater than I – white. The result of such a transformation of the grey image into a black-and-white image is presented in Figs 6a, b (the size of each pattern is 40 × 40 μm). The black image areas correspond to the pores, whilst the white image areas – to the skeleton of a porous sample.

At the second stage, the fractal dimension was determined by the formula [25]

$$D = \lim_{\delta \to \infty} \frac{\ln L}{\ln \delta} + 1, \quad (7)$$

where L is the number of filled cells for a given partition; and δ is the number of the square side's partitions (δ^2 is the number of cells for a given partition). Tot this end, a uniform regular grid with a given amount of square cells (Fig. 6b) was superimposed upon the resulting black-and-white image of

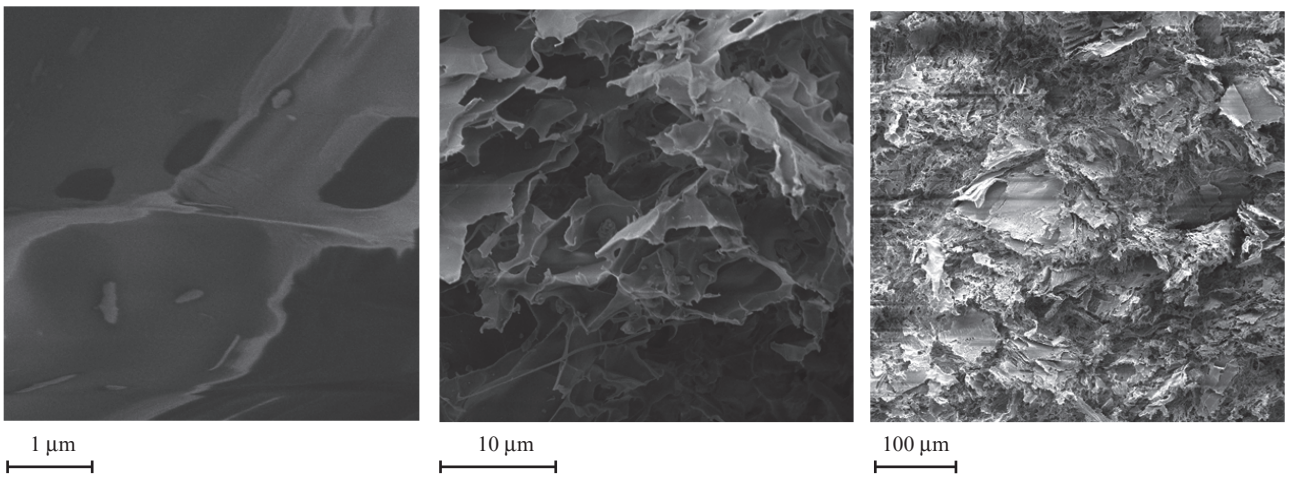

Figure 5. Micro-images of the sample surface at various magnifications.

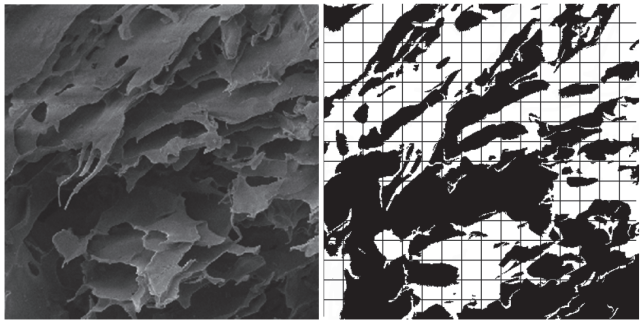

Figure 6. Micro-images of the sample surface in (a) grey and (b) black-and-white colour. The image partition parameter δ = 16.

the sample. Next, the number of filled cells for each value of threshold brightness, varying from 10 to 250, was determined. The procedure was conducted in the following way. The average brightness value was calculated for each particular cell and minimal threshold brightness was assigned to that cell; in this case, the average brightness of the cell turns out higher than the minimal one. Then, for each value of threshold brightness, the number L of corresponding cells and the ratio $D_a = \ln L/\ln\delta$ were calculated. After that the mesh size was reduced so that the parameter δ became two-fold decreased compared to the previous value, and the above-described procedure was repeated. Figure 7 shows a typical group of dependences of the ratio D_a on the control value of brightness for the partition parameters δ = 4, 8, 16, ... 256, and 768. Having chosen the value of D_a as an average value calculated over the linear part of each curve, we obtained the dependence of D_a on the partition parameter δ (Fig. 8). The value $D = D_a + 1$, with δ tending to infinity, was used as the fractal dimension.

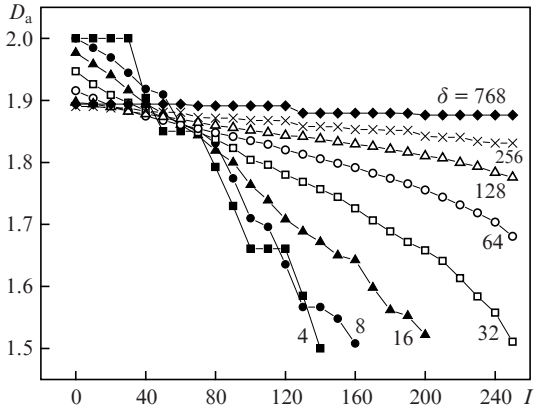

Figure 7. Dependence of the value D_a on the brightness criterion I for different values of the partition parameter δ.

A similar procedure was performed for all six samples with the use of several images obtained for the same sample at different magnifications, the magnifications for the first and last images differing by 200 times. The average value of the fractal dimension for all images of the samples constituted 2.85 ± 0.02. For some porous samples, the fractal dimension cannot be defined using the algorithm described, which means

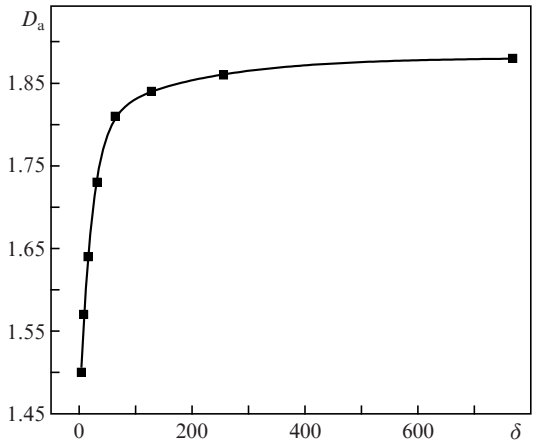

Figure 8. Dependence of D_a on the partition parameter δ.

that the relevant structure does not possess a fractal character.

4. Relationship between the fractal dimension and the alpha-particle path length distribution in the structure of porous samples

The size distribution of the number of substance grains in foams for fractal structures is given by the expression [25, 19]

$$n(\rho) \approx a\rho^{-D}, \tag{8}$$

where $\rho = r/h$; r is the grain size; h is the sample height (in the direction of alpha-particle beam propagation); and a is the normalisation factor. The relative density of grains, the size of which is confined in the interval from ρ to $\rho + d\rho$ in the sample with volume V_0, appears as

$$\frac{dV_\rho}{V_0} \sim \frac{\rho^3 n(\rho)}{V_0} d\rho. \tag{9}$$

The probability for the alpha-particle trajectory to hit a grain of size ρ can be calculated as

$$\frac{S_\rho}{S_0} \sim \frac{\rho^2}{S_0}, \tag{10}$$

where S_0 is the sample base area. The grain size distribution of the alpha-particle trajectories, $p_s(\rho)d\rho$, is determined by the product of the grain density by the probability for the trajectory to hit a grain:

$$p_s(\rho)d\rho \sim \rho^{5-D} d\rho. \tag{11}$$

The relationship between the thickness of grains in a substance and their size is defined by the expressions

$$ds \sim \rho n(\rho) d\rho, \quad s(\rho) \sim \int_\rho^1 \rho n(\rho) d\rho = a\frac{1-\rho^{2-D}}{2-D}, \tag{12}$$

where the value of s is normalised to mh (m is the substance density of foam grains). To obtain the path length distribution in the foam substance, we need to express ρ through s and $d\rho$ through ds:

$$\rho \sim \left(1 + \frac{D-2}{a}s\right)^{\frac{1}{2-D}},\ \mathrm{d}\rho \sim \left(1 + \frac{D-2}{a}s\right)^{\frac{D-1}{2-D}}\mathrm{d}s. \qquad (13)$$

After substituting (13) into (11), we have

$$p(s)\mathrm{d}s \sim \left(1 + \frac{D-2}{a}s\right)^{\frac{4}{2-D}}\mathrm{d}s. \qquad (14)$$

The value of the coefficient a is estimated from the normalisation condition

$$a\int_{\rho_{\min}}^{1}\frac{\mathrm{d}\rho}{\rho^{D}} = a\frac{1-\rho_{\min}^{1-D}}{1-D} = 1, \qquad (15)$$

and, provided that $\rho_{\min} \ll 1$, we obtain $a \approx (D-1)\rho_{\min}^{D-1}$. Now distribution (14) can be written as

$$p(s)\mathrm{d}s \sim \left(\frac{D-2}{D-1}\rho_{\min}^{1-D}s\right)^{\frac{4}{2-D}}\mathrm{d}s = bs^{\frac{4}{2-D}}\mathrm{d}s. \qquad (16)$$

As mentioned above, the fractal dimension of our foam $D = 2.85$. Then $p(s) = b/s^{4.7}$. The distribution function $p(s)$ (16) is shown in Fig. 9 [curve (*3*)] together with the path length distribution $\varphi(s)$ of alpha-particles in the porous sample skeleton, obtained from the alpha-particle energy spectrum. The value b (or $\rho_{\min}$) is selected so that the curve $p(s)$ be tangent to the curve $\varphi(s)$.

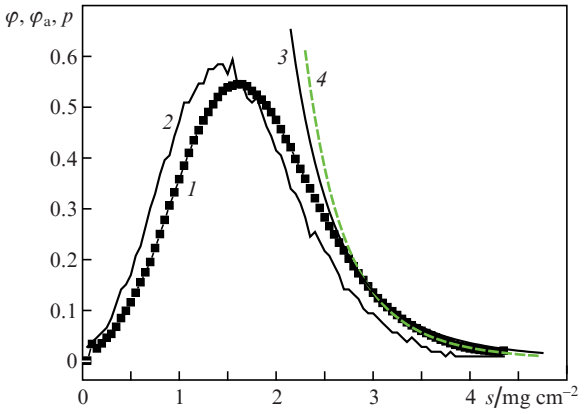

Figure 9. Optical path length distributions of the trajectories for a porous sample: (*1*) distribution $\varphi(s)$ obtained from the alpha-particle spectrum with regard to straggling, source spectrum, and hardware broadening [formula (1)], (*2*) distribution $\varphi_a(s)$ obtained from the alpha-particle spectrum with regard to energy losses only [formula (5)], (*3*) distribution $p(s)$ obtained from the fractal image analysis [formula (14)] and (*4*) the power law $p(s) = b/s^{4.7}$.

One might expect that curve (*3*) will be good to describe the descending part of dependence (*1*). However, this region can be in the best way approximated by the power law $p(s) = b/s^{4.7}$ [curve (*4*)]. The discrepancy can be explained by anisotropy of the foam structure consisting of the randomly oriented film-type formations and also by an inaccuracy in the D value evaluation. For our conditions, the assessment of the minimum grain size affecting the distribution of the number of trajectories by the skeleton length at $s \approx 2.8-4.5$ mg cm^{-2} gives $\rho_{\min} \approx 0.01$ (or $r \sim 10^{-4}$ cm).

In the framework of the above-described formalism, an estimate of the average grain size appears as

$$\bar{\rho} \approx \int_{\rho_{\min}}^{1}\rho n(\rho)\mathrm{d}\rho \approx \frac{D-1}{D-2}\rho_{\min}. \qquad (17)$$

The total volume of grains (skeleton substance) is determined as

$$V_s \approx \int_{\rho_{\min}}^{1} s^3(\rho)n(\rho)\mathrm{d}\rho \approx \frac{(D-1)^4}{(D-2)^3(4D-7)}\rho_{\min}^3, \qquad (18)$$

where $s(\rho)$ is taken in the form of (12). It is here assumed that $\rho_{\min} \ll 1$. Passing over from dimensionless values to dimensional ones, from (17) and (18) we obtain a relationship between the average grain size $\bar{r}$ and the volume V_s of the skeleton substance in the form

$$\frac{\bar{r}}{h} \approx \left(\frac{4D-7}{D-1}\frac{V_s}{V_0}\right)^{1/3}. \qquad (19)$$

If we assume that the thickness h of the foam sample is proportional to the average pore size d_0, whilst the foam volume is approximately equal to the volume of pores, the ratio of the average size of grains in the skeleton and pores as a function of the ratio of the total volume of grains in the skeleton and pores takes the form $\bar{r}/d_0 \sim (V_s/V_0)^{0.33}$. This is not consistent with a similar ratio in [10, 11], where the exponent is assumed to be 0.8. The difference is caused by different definitions of the sizes of a pore and a grain. In [10, 11] the ratio $\bar{r}/d_0$ is considered as a ratio of the thickness to the length of membranes or filaments that make up the foam skeleton. In this paper it is the ratio of the average grain size of the skeleton and pores. Herewith, the grain size is treated not as a specific size in a particular porous structure, but as a size determined by statistical processing in the approximation of fractal clusters.

5. Conclusions

Thus, the alpha-spectrometry method, in addition to the integrity control and evaluation of the thickness nonuniformity in the film-type samples, can be applied to obtain the path length distribution of alpha-particles in the substance of the skeleton. The analysis of micro-images of the slices of porous samples has shown that their structure has a fractal nature on the relative scale of magnifications in the range of 1–200; fractal dimension of the skeleton grains has been determined. The path length distribution in the skeleton derived using the fractal dimension is close to that obtained from the alpha-spectra in the right descending part of the distribution. This gives reason to assume that the grain size distribution in the low-porosity areas has a form of ρ^{-D}, being characteristic of fractal structures. These data can be used as a source in theoretical consideration of propagation of laser and X-ray radiation in specific porous samples.

References

1. Lindl J. *Phys. Plasmas*, **2**, 3933 (1995).
2. Bugrov A.E., Burdonskii I.N., Gavrilov V.V., Gol'tsov A.Yu., Gus'kov S.Yu., Zhuzhukalo E.V., Kovalskii N.G., Pergament M.I., Petryakov V.M., Rozanov V.B. *Zh. Eksp. Teor. Fiz.*, **111**, 903 (1997).
3. Khalenkov A.M., Borisenko N.G., et al. *Laser Part. Beams*, **24**, 283 (2006).
4. Nuckolls J.H., Thiessen A.R., Dahlbacka G.H. US Patent 4376752 (1983).
5. Gus'kov S.Yu., Zmitrenko N.V., Rozanov V.B. *Zh. Eksp. Teor. Fiz.*, **108**, 548 (1995).
6. Koch J.A., Esrtebrook K.G., Bauer J.D., et al. *Phys. Plasmas*, **2C**, 3820 (1995).

7. Dresselberger M., Jones M.W., Edwards J., Dunne M., Willi O. *Phys. Rev. Lett*., **74**, 2961 (1999).
8. Garanin S.G., Derkach V.N., Shnyagin R.A. *Kvantovaya Elektron*., **34**, 427 (2004) [*Quantum Electron.*, **34**, 427 (2004)].
9. Depierreux S., Labaune C., Michel D.T., Stenz C., Nicolaï P., Grech M., Raizuelo G., Weber S., Riconda C., Tikhonchuk V.T., Loiseau P., Borisenko N.G., Nazarov W., Huller S., Pesme D., Casanova M., Limpouch J., Meyer C., Di-Nicola P., Wrobel R., Alozy E., Romary P., Thiell G., Soullie G., Reverdin C., Villette B. *Phys. Rev. Lett*., **102**, 195005 (2009).
10. Gus'kov S.Yu. *J. Russ. Laser Res*., **31**, 574 (2010).
11. Gus'kov S.Yu., Limpouch J., Nikolaï Ph., Tikhonchuk V.T. *Phys. Plasmas*, **18**, 103114 (2011).
12. Borisenko N.G., Merkul'ev Yu.A., Orekhov A.S., Chaurasiya Sh., Tripathi S., Munda D.S., Gupta N.K., Darishvar L.J., Pimenov V.G. *Fiz. Plasmy*, **38** (8), 752 (2013).
13. Ge L., Nagai K., Njrimatsu T., et al. *J. Phys. Conf. Ser*., **112**, 032065 (2008).
14. Gus'kov S.Yu., Merkul'ev Yu.A. *Kvantovaya Elektron*., **31**, 311 (2001) [*Quantum Electron.*, **31**, 311 (2001)].
15. Rosen M.D., Hammer J.H. *Phys. Rev. E*, **72**, 056403 (2005).
16. Borisenko N.G., Gromov A.I., Merkul'ev Yu.A., Orekhov A.S., Chaurasiya Sh., Tripathi S., Munda D.S., Gupta N.K., Darishvar L.J. Preprint FIAN, No. 29 (Moscow, 2011).
17. Koenig M., Bondenne J.M., Batini D., Benuzzi A., Bossi S., Temporal M., Atzeni S. *Phys. Rev. Lett*., **74**, 2260 (1995).
18. Schmidt F.K. *Fraktalnyi analiz v fiziko-khimii geterogennykh system i polimerov* (Fractal Analysis in Physical Chemistry of Heterogeneous Systems and Polymers) (Irkutsk: 'Irkutsk University', 2001).
19. Mosolov A.B., Dinariev O.Yu. *Zh. Tekh Fiz*., **58**, 233 (1988).
20. Akimova I.V., Borisenko N.G., Gromov A.I., Merkul'ev Yu.A., Orekhov A.S. *VANT. Ser. Termoyad. Sintez*, (2), 122 (2012).
21. Izgorodin V.M., Abzaev F.M., Balyaev A.P., Bessarab A.V., Cherkesova I.N., Chulkov V.V., Fenoshin D.Yu., Garanin S.G., et al. *Laser Part. Beams*, **27**, 657 (2009).
22. Landau L. *J. Phys*., **8**, 201 (1944).
23. Comfort J.R., Decker J.F., Link E.T., Scully M.O., Quinton A.R. *Phys. Rev*., **150**, 249 (1966).
24. Gnedenko B.V. *Kurs teorii veroyatnostei* (The Course of Probability Theory) (M.: 'Nauka', 1965).
25. Mandelbrot B.B. *The Fractal Geometry in Nature* (San-Francisko: W.N. Freeman, 1982).
26. Yablokov M.Yu. *Zh. Fiz. Khim*., **73**, 214 (1999).